PHYSICAL REVIEW B **93**, 205122 (2016)

# Thermally activated heavy states and anomalous optical properties in a multiband metal: The case of $SrMnSb_2$

H. J. Park,[1,2] Luke J. Sandilands,[1,2] J. S. You,[3] Hyo Seok Ji,[4] C. H. Sohn,[1,2] J. W. Han,[5] S. J. Moon,[6] K. W. Kim,[7] J. H. Shim,[4,8] Jun Sung Kim,[3] and T. W. Noh[1,2,*]

[1]*Center for Correlated Electron Systems, Institute for Basic Science (IBS), Seoul 151-742, Republic of Korea*
[2]*Department of Physics and Astronomy, Seoul National University (SNU), Seoul 151-742, Republic of Korea*
[3]*Department of Physics, Pohang University of Science and Technology, Pohang 790-784, Republic of Korea*
[4]*Department of Chemistry, Pohang University of Science and Technology, Pohang 790-784, Republic of Korea*
[5]*Department of Physics and Photon Science, School of Physics and Chemistry, Gwangju Institute of Science and Technology (GIST), Gwangju 500-712, Republic of Korea*
[6]*Department of Physics, Hanyang University, Seoul 133-791, Republic of Korea*
[7]*Department of Physics, Chungbuk National University, Cheongju 361-763, Republic of Korea*
[8]*Division of Advanced Nuclear Engineering, Pohang University of Science and Technology, Pohang 790-784, Republic of Korea*

(Received 13 October 2015; revised manuscript received 3 March 2016; published 13 May 2016)

We report an optical spectroscopic study of $SrMnSb_2$, a low-carrier-density metal. As temperature is decreased, our measurements reveal a large increase in the quasiparticle plasma frequency, which is highly unusual for a metal. This seemingly anomalous behavior can be accounted for using a "three-band" model of the multiband electronic structure of $SrMnSb_2$ that includes two conduction bands and one valence band. The second conduction band is assumed to be heavy and its minimum is taken to be close to, but not intersecting, the Fermi level. At finite temperature, quasiparticles are thermally redistributed between the two conduction bands, leading to an increase in the optical effective mass and a decrease in the plasma frequency. The temperature dependence of the low-lying interband optical transitions and the Hall number can also be understood using our model. The phenomenology of such a three-band scenario has not been widely considered to date in optical spectroscopic studies. Our results provide an explanation for the puzzling optical properties that have previously been reported in a number of topical low-carrier-density metals and semimetals and lay a foundation for future optical studies of these materials.

DOI: 10.1103/PhysRevB.93.205122

## I. INTRODUCTION

Recently, there has been a spate of investigations into low-density metals or semimetals with multiband electronic structures, as these compounds are known to display intriguing physics. Due to high characteristic mobilities, multiple species of charge carriers, and, in some cases, novel electronic dispersions, these materials reveal a variety of spectacular transport properties and/or quantum states that have not been observed in conventional metals or insulators. The semimetals bismuth and graphite, for instance, reveal novel magnetotransport effects and broken symmetry states at high fields [1,2]. As a result, low-density electron-hole systems have historically attracted significant interest, with the discoveries of graphene and of topological insulators adding further impetus to the field [3,4]. Very recently, attention has focused on bulk materials hosting relativistic Dirac or Weyl fermions [5,6]. These systems are characterized by linearly dispersing bands near the Fermi level and topologically nontrivial semimetallic band structures [7]. Accordingly, a number of exceptional features are anticipated, including Fermi "arc" surface states and novel transport effects [8], some of which may have already been observed [9–11]. Multiband systems can also host unorthodox quantum states, including excitonic insulating [12] or superconducting states [13]. In the Fe-based superconductors, for instance, the multiband electronic structure is thought to play an important role in realizing unconventional superconductivity [13]. Recent studies have also revealed that Fe(Te,Se) might exhibit a Bardeen-Cooper-Schrieffer (BCS) to Bose-Einstein condensate (BEC) crossover due to the presence of multiple bands with very small Fermi energy [14,15].

Multiband systems also tend to display anomalous changes in the electronic response with variation of temperature, even in the absence of phase transitions. In conventional metals, the Fermi energy ($E_F$) is of order of a few eV and the density of states [$D(E)$] is considered to be constant within $k_BT$ (the thermal energy scale) of $E_F$. Thermal effects therefore do not significantly affect the electron occupancy. Similarly, insulators with energy gaps large compared to $k_BT$ do not show a strong temperature dependence. In contrast, many low-carrier-density, multiband systems display unusual temperature-dependent properties. In particular, an anomalous increase in the plasma frequency ($\omega_p$) with decreasing temperature has been observed in multiband and/or low-carrier-density systems such as $Cu_xTiSe_2$ [16], several topological insulator systems [17,18], lead chalcogenide thermoelectric alloys [19,20], and $LaTiO_3/SrTiO_3$ superlattices [21]. It should be stressed that the multiband nature and the shallowness of the electron/hole pockets are key ingredients for realizing exotic phenomena in semimetallic compounds. A detailed understanding of the link between transport/optical properties and electronic structure in multiband systems is therefore crucial.

Optical spectroscopy is a ubiquitous and powerful technique for studying the electronic structure of solids [22,23].

*twnoh@snu.ac.kr

 

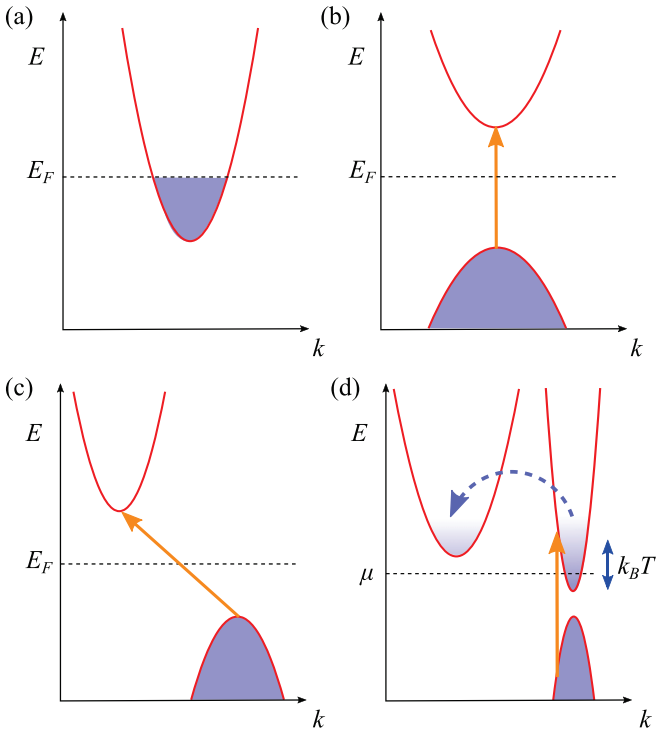


FIG. 1. Schematic band structures for (a) single band metal, (b) direct gap insulator, (c) indirect gap insulator, and (d) multiband metal. The occupied states are shown in purple, while the lowest energy interband optical transitions are shown with orange arrows. In (d), thermal activation (indicated with the dashed blue arrow) between conduction bands is expected to affect the optical properties.

However, the multiband materials discussed above present a challenge to optical spectroscopy, which is a momentum averaged probe [24–26]. Conventional explanations of the optical response of solids are based on either the electrodynamics of a single band or on optical transitions between two bands. For a metal, the optical properties are usually described by the electrodynamic response of free carriers in a single band, as shown in Fig. 1(a). For an insulator, depending on the nature of the gap, the optical properties are typically discussed in terms of either direct or indirect optical transitions between conduction and valence bands [see Figs. 1(b) and 1(c)]. However, such simple descriptions are not expected to be sufficient when several conduction and/or valence bands contribute to the optical response.

Indeed, multiband effects might be expected to significantly affect the optical properties. One such multiband scenario is illustrated in Fig. 1(d), where an additional conduction band is located near $E_F$. Provided $k_BT$ is comparable to the band separation, a thermal redistribution of carriers between bands should occur. In the particular example of Fig. 1(d), a thermal redistribution is anticipated between the two conduction bands. Additionally, if the effective masses of the relevant bands differ significantly, this redistribution should also produce changes in the transport and optical properties that are sensitive to the effective mass. One example quantity is the optical plasma frequency which is inversely related to the effective mass [22]. To the best of our knowledge, the effects of such thermal redistribution on the optical response have not been widely considered in existing optical studies, with the exception of PbTe [27]. We believe that a proper treatment of this possibility can shed light on certain unresolved problems in the study of multiband metals, specifically reports of anomalous changes in $\omega_p$ observed in a number of low-carrier-density systems [16–18,21].

In this context, $SrMnSb_2$ is an ideal model system to investigate the effects of the multiband nature and shallowness of the electron/hole pockets on the transport and optical properties. $SrMnSb_2$ is structurally similar to $SrMnBi_2$ and $CaMnBi_2$, which are known to feature anisotropic Dirac fermions [28,29]. Crystallographically, these materials feature stacked structures made up of MnBi, Sr (Ca), and Bi square net layers [30,31] and are structurally similar to some pnictide superconductors [32]. Strong correlation in the Mn $3d$ states means these bands are far from the Fermi level ($E_F$) and the electronic conduction is dominated by the Bi layers [28]. Detailed studies have demonstrated that the Bi square nets host highly anisotropic two-dimensional (2D) Dirac fermions [28,29,31,33,34]. In $SrMnSb_2$, on the other hand, the orthorhombic distortion of the crystal structure removes the Dirac points and results in several conventional parabolic bands near $E_F$ [35]. The relative simplicity of the band structure makes $SrMnSb_2$ an ideal prototype for exploring the transport properties of low-carrier-density, multiband metals.

In this work, we report on the optical and transport properties of $SrMnSb_2$. Our measurements reveal a number of unusual phenomena, in spite of the simple electronic structure. In particular, we observe an anomalously large *increase* in the optical plasma frequency ($\omega_p$) with decreasing temperature ($T$), which is very unusual in simple metallic systems. To explain the anomalous optical properties of $SrMnSb_2$, we develop a three-band description. In the case of $SrMnSb_2$, we consider two electronlike bands and one holelike band, as illustrated schematically in Fig. 1(d). By accounting for the thermal redistribution of quasiparticles between these bands, this simple model can explain the $T$ dependence of $\omega_p$, the optical interband transitions, and the Hall number. Using this three-band model, we also extracted detailed information on the band structure from the momentum-averaged optical/transport data that agrees well with theoretical expectations. Our results clearly illustrate the phenomenology associated with an additional conduction band near $E_F$ and demonstrate that a detailed understanding of the low-energy electronic structure in a multiband system can be obtained by careful consideration of the $T$-dependent optical response. We suggest that the three-band description described here should be broadly relevant to interpreting the transport and optical properties of other low-carrier-density metals with multivalley electronic structures.

## II. EXPERIMENTAL DETAILS AND RESULTS

### A. Optical measurements

To determine the complex optical conductivity $\tilde{\sigma}(\omega)$ of $SrMnSb_2$, we performed spectroscopic reflectance and ellipsometry measurements. Single crystals of $SrMnSb_2$ were grown using Sn flux. The high crystallinity and stoichiometry were confirmed by x-ray diffraction and energy dispersive x-ray spectroscopy, respectively. The optical measurements

were performed on a cleaved surface of a (001) plane. From 0.74 to 5.0 eV, we directly measured the $T$ dependence of $\tilde{\sigma}(\omega)$ using a commercial ellipsometer (J. A. Woollam, V-VASE) from 10 to 300 K. From 0.008 to 0.8 eV, we measured the reflectance spectra $[R(\omega)]$ using a Fourier transform infrared (FTIR) spectrometer (Bruker IFS 66v/S). We employed the *in situ* gold coating method to obtain properly normalized $R(\omega)$ spectra that are free of possible errors from geometric effects [36]. The sample $T$ was varied from 10 to 350 K using a continuous flow liquid He cryostat with the sample in vacuum.

We performed Kramers-Kronig (KK) analysis to obtain $\tilde{\sigma}(\omega)$ from the $R(\omega)$ data. This analysis requires that $R(\omega)$ be known over a broad energy range, so we extended $R(\omega)$ below 0.008 eV using the standard Hagen-Rubens relation [22]. At energies above 0.8 eV, we computed $R(\omega)$ from the ellipsometric data. Between our upper cutoff of 5 and 12 eV, we extrapolated $R(\omega)$ by assuming $R(\omega) \propto \omega^{-1}$. Above 12 eV, $R(\omega)$ was assumed to decrease as $\omega^{-4}$. The region below 0.5 eV, which we focus on in this work, is not affected by the choice of extrapolation above 5 eV. The KK-derived $\tilde{\sigma}(\omega)$ were found to be in good agreement with the ellipsometric data, validating our analysis.

As a complementary probe of the electronic structure, we also measured the longitudinal and Hall resistivity ($\rho_{xx}$ and $\rho_{xy}$) as a function of magnetic field ($B$) at various $T$ between 2 and 300 K. The data were measured using the standard six-probe method in a Physical Property Measurement System (PPMS-14T, Quantum Design). For the dc measurements, we used a crystal from the same batch as the sample used in the optical experiment. For precise determination of the Hall coefficient, we recorded the Hall voltages at a fixed $T$ by sweeping the magnetic field between $-14$ and 14 T and subtracted the asymmetric component due to contact misalignment.

### B. Quantifying the optical response of $SrMnSb_2$

Although $SrMnSb_2$ remains metallic in the investigated temperature window, the $R(\omega)$ data show an unusually large $T$ dependence. As shown in Fig. 2(a), $R(\omega)$ approaches 1 at low energies for all $T$, typical for a metal. At higher energies, $R(\omega)$ decreases, reaching a well-defined plasma minimum near 90 meV at 300 K. As $T$ is decreased, the data in Fig. 2(a) reveal a large and remarkable change in $R(\omega)$. In particular, the plasma edge sharpens and shifts to higher frequency, reaching 130 meV at 10 K. The data of Fig. 2(a) therefore suggest a collapse of the scattering rate $1/\tau$ and a significant change in the charge dynamics. A reduction in $1/\tau$ can be easily anticipated as $T$ is decreased. However, the blueshift of the plasma minimum is highly unusual in a typical metal.

Within the single-band Drude model, the location of the plasma minimum is given by the screened plasma frequency $\omega_p^{*2} = \omega_p^2/\varepsilon_\infty = 4\pi e^2 n/m_b\varepsilon_\infty$, where $n$ is the carrier density, $m_b$ the optical effective mass, and $\varepsilon_\infty$ is the dielectric screening parameter (see Appendix A for further information) [22]. In a typical metal, where $E_F$ is much larger than $k_BT$ and $D(E)$ does not vary strongly near $E_F$, $\omega_p$ (and $\omega_p^*$) should be nearly independent of $T$. Indeed, Au shows a $T$-dependent blueshift of $\omega_p$ on the order of 1% [37]. To the best of our knowledge, a $T$-dependent $\omega_p$, such as we observe in $SrMnSb_2$, has rarely been found in the absence of strong electron-electron interactions and is considered highly anomalous. Specific materials exhibiting such a peculiar $\omega_p$ shift include $Cu_xTiSe_2$, certain topological insulator systems, and LTO/STO superlattices [16–18,21].

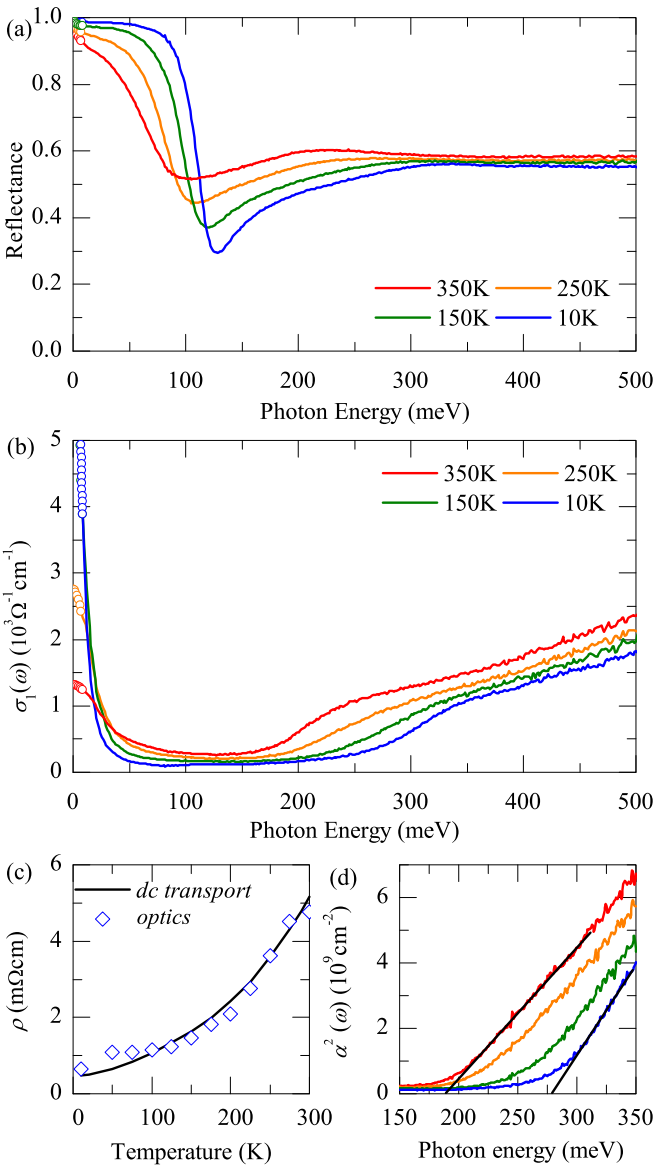


FIG. 2. (a) Reflectance $[R(\omega)]$ and (b) optical conductivity $[\sigma_1(\omega)]$ of $SrMnSb_2$. Both $R(\omega)$ and $\sigma_1(\omega)$ reveal large changes with $T$. (c) Optical resistivity $[\lim_{\omega\to 0} 1/\sigma_1(\omega)]$ and dc resistivity. (d) Square of the absorption $[\alpha(\omega)]$ and the linear extrapolations used to estimate the direct gap $E_g$.

The anomalous charge dynamics are evident in the optical constants derived by KK transformation of $R(\omega)$. In the low-frequency region below 100 meV, the optical conductivity $\sigma_1(\omega)$ shown in Fig. 2(b) is dominated by a narrow quasiparticle (Drude) peak centered at zero frequency. The open diamonds in the Fig. 2(c) show the dc limit values of $1/\sigma_1(\omega)$. The solid line shows the measured dc electrical resistivity curve multiplied with a factor of 0.75. Considering sample variation, geometrical factors due to sample shape,

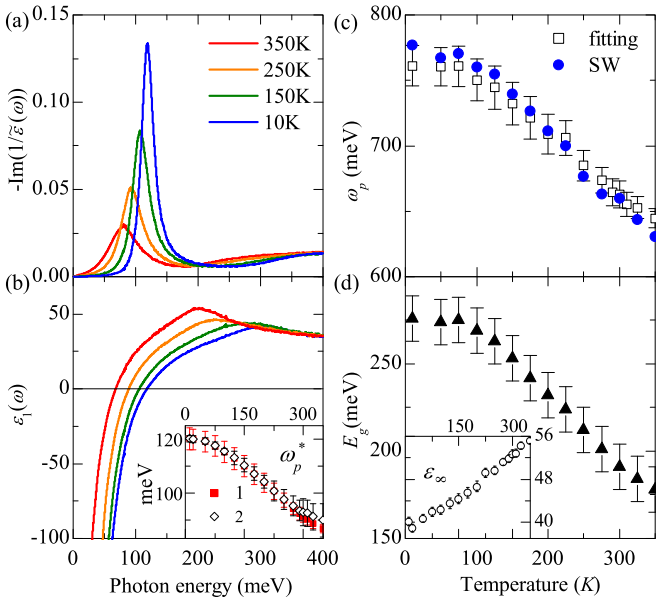


FIG. 3. (a) Energy loss function [Im$(-1/\varepsilon)$], (b) Real part of the dielectric function ($\varepsilon_1$), (c) plasma frequency ($\omega_p$), and (d) gap parameter ($E_g$) of $SrMnSb_2$. The inset of (b) shows the $T$ dependent screened plasma frequency ($\omega_p^*$) obtained from (1) fitting and (2) compensated zero crossing of $\varepsilon_1$. The inset of (d) shows dielectric screening parameter $\varepsilon_\infty$.

and contact layer, the dc limit value of the KK analysis agrees reasonably with the measured dc data. As $T$ increases, the Drude peak strength seems to decrease but its width seems to increase. The decrease of Drude weight suggests that $\omega_p^*$ should decrease, which was already evident from the $R(\omega)$ spectra.

In addition, we investigated the loss function spectra Im$(-1/\varepsilon)$ and the real part of the dielectric function $\varepsilon_1(\omega)$ to obtain further confirmation on the anomalous charge dynamics of $SrMnSb_2$. Within the Drude model, $\varepsilon_1(\omega)$ becomes zero near the screened plasma frequency $\omega_p^*/\omega_p\varepsilon_\infty^{1/2}$, while Im$(-1/\varepsilon)$ shows a peak structure at $\omega_p^*$ (see Appendix A for further details). As can be seen in Figs. 3(a) and 3(b), the $\varepsilon_1(\omega)$ data indeed show a zero crossing, while Im$(-1/\varepsilon)$ peaks at the same frequency. Both the zero crossing in $\varepsilon_1(\omega)$ and the peak structure in Im$(-1/\varepsilon)$ shift to higher energies at low $T$, confirming the strong blueshift of $\omega_p^*$ implied by the $R(\omega)$ data. The inset of Fig. 3(b) shows that the $\omega_p^*$ values from the Im$(-1/\varepsilon)$ peak position are consistent with those from the $\varepsilon_1$ zero crossing.

To quantify the $T$ dependence, we fitted our $\varepsilon_1(\omega)$ and Im$(-1/\varepsilon)$ data with the standard Drude model (see Appendix A for details). The resulting bare plasma frequency ($\omega_p$) and dielectric screening parameter ($\varepsilon_\infty$) values are shown in Fig. 3(c) and the inset of Fig. 3(d), respectively. Note that $\varepsilon_\infty$ gradually increases as $T$ is raised. Consistent with our earlier discussion, $\omega_p$ reveals a noticeable temperature dependence, increasing by 19% from 300 to 10 K. We could also obtain $\omega_p$ by integrating the spectral weight (SW) of the Drude peak, i.e., $\sigma_1(\omega)$ from 8 to 170 meV. As shown in Fig. 3(c), the results from the sum rule analysis agree with the fitting results. This figure demonstrates an increase in the

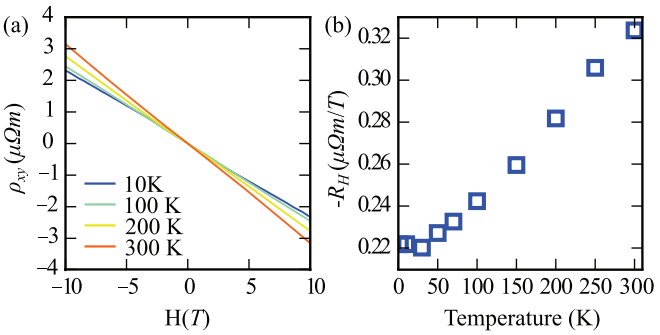


FIG. 4. (a) Field-dependent Hall resistivity ($\rho_{xy}$) and (b) the Hall number ($R_H$). The Hall data show a substantial $T$-dependence.

bare plasma frequency $\omega_p$ at low temperatures (rather than $\omega_p^*$ only) and signals a pronounced and unexpected change in the quasiparticle dynamics. The spectral weight lost from the Drude peak at high temperatures is recovered by about 250 meV (see Appendix B).

In addition to the anomalous change of $\omega_p$, the $\sigma_1(\omega)$ spectra reveal another aspect of the low-energy-charge dynamics. Near 200 meV, $\sigma_1(\omega)$ shows a gaplike structure corresponding to the onset of interband transitions. The inset of Fig. 2(d) shows that $\alpha^2(\omega) \propto (\hbar\omega - E_g)$, which demonstrates that the gaplike structure originates from direct optical transitions across an optical energy gap $E_g$. Figure 3(d) shows that $E_g$ increases with decreasing $T$. The increase in $E_g$ is consistent with the decrease in $\varepsilon_\infty$ described earlier. By moving to higher energies, the interband transitions become less effective in screening low-energy-charge excitations, leading to a reduction in $\varepsilon_\infty$.

To gain further insight into the anomalous properties of $SrMnSb_2$, we now turn to the Hall data. Figure 4 reveals that the Hall data also show significant $T$ dependence. Since $\rho_{xy}$ was found to be a quasilinear function of $B$ at all $T$ [Fig. 4(a)], we could extract the Hall number ($R_H$) as a function of $T$ through a linear fit of $\rho_{xy}(B)$. The $R_H$ values are shown in Fig. 4(b). At low $T$, $R_H$ is relatively constant with a value of $-0.22\,\mu\Omega$ m/T, implying a Hall density ($n_H$) of $2.84 \times 10^{19}$ cm$^{-3}$ and electronlike quasiparticles. As $T$ increases, $R_H$ decreases monotonically, reaching a value of $-0.323\,\mu\Omega$ m/T at 300 K. At 10 K, $n_H$ is 45% larger than the 300 K value, comparable to the 37% increase in $\omega_p^2$ over the same $T$ range. Within a single-band model, this would imply a highly unusual *decrease* in the number of quasiparticles with increased $T$. However, as we shall argue later, the peculiar $T$ dependence of the optical response and $R_H$ is a consequence of the multiband electronic structure, and hence highly structured density of states $D(E)$, of $SrMnSb_2$.

## III. DISCUSSION

As mentioned earlier, large changes in $\omega_p$ have only been observed in a limited number of materials. This unusual behavior has usually been associated with exotic electronic behavior such as strong correlations in the high-$T_c$ cuprates and iron chalcogenides [37,38], "quasiparticle undressing" in $EuB_6$ [39,40], ferromagnetism in (Ga,Mn)As [41], or the anomalous metallic state in $Cu_xTiSe_2$ [16]. However, strong correlations and/or magnetism are unlikely to affect $\omega_p$ in

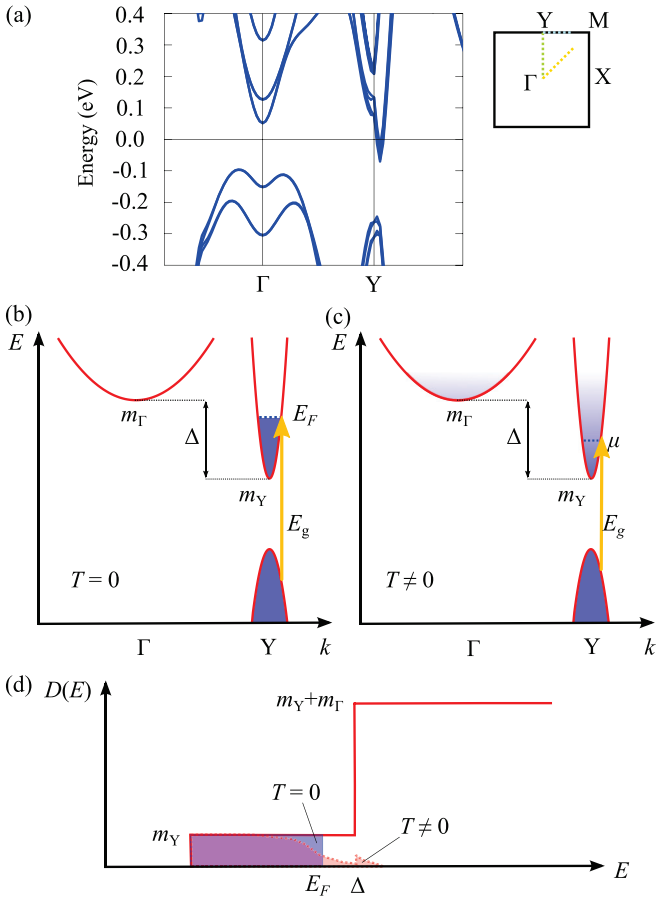


FIG. 5. (a) The *ab initio* band structure near $E_F$ and 2D schematic of the Brillouin zone (BZ) in the $k_z = 0$ plane. The band structure is calculated along the high symmetry lines shown in the schematic BZ. Schematic diagrams of the three-band model in (b) low $T$ and (c) high $T$ cases. (d) The density of states [$D(E)$] for the three-band model. Panel (a) is reproduced from Ref. [35] with $E_F$ adjusted to match the Hall data. In (b)–(d), the state occupancy is indicated in blue, while possible optical direct transitions are marked with yellow arrows. The conduction band offset ($\Delta$) and masses ($m_\Gamma$ and $m_Y$) are also marked in (b) and (c).

the present case. In $SrMnSb_2$, the electronic states near $E_F$ are predominantly derived from Sb orbitals and electronic correlations are not expected to be strong [35]. This conclusion is supported by the conventional Drude line shape seen in the optical response, as strong correlations tend to produce a non-Drude line shape [23]. Although the Mn moments in $SrMnSb_2$ order antiferromagnetically near 300 K [42], the localized Mn states relevant to the magnetism are thought to be far from $E_F$ [35] and our data show no noticeable anomaly near $T_N$. Therefore, strong correlations and/or magnetism cannot explain the anomalous blueshift of $\omega_p$, and we are forced to consider other possibilities.

Previous *ab initio* work has demonstrated that $SrMnSb_2$ possesses a multiband electronic structure near $E_F$ [35]. A 2D projection of the Brillouin zone suitable to $SrMnSb_2$ and the result of these calculations are reproduced in Fig. 5(a). Several bands with quasi-2D dispersions are found near $E_F$. In particular, a group of light (heavy) electron and hole bands are located near Y(Γ) [35]. Meanwhile, the Hall data indicate $SrMnSb_2$ is a low-carrier-density metal with $n_H = 2.84 \times 10^{19}\,\mathrm{cm}^{-3}$ and electronlike quasiparticles at low $T$, consistent with quantum oscillation and thermoelectric measurements [42]. Assuming that the quasiparticles occupy a single, 2D band near Y at low $T$, we can combine $n_H$ with the 10 K plasma frequency to estimate $m_Y = 0.069\,m_e$ and $E_F = 116\,\mathrm{meV}$. Importantly, the edge of the heavier Γ band is then expected only slightly above $E_F$. As a result, the energy difference between the $E_F$ and the Γ band edge is on the order of 10 meV, which produces the large change in $\omega_p$ via a thermal redistribution of carriers between the conduction bands at Y and Γ.

Motivated by the *ab initio* band structure, we now consider the effects of thermal redistribution between multiple near-$E_F$ bands on the optical response of $SrMnSb_2$. As emphasized earlier, $SrMnSb_2$ has two intriguing properties, i.e., the anomalous shift of $\omega_p$ and $R_H$ with $T$. These properties are difficult to reconcile with optical processes in a single conduction band. By considering the thermal activation of a second, heavy conduction band at Γ, we can successfully account for the $T$ dependence of $\omega_p$, $R_H$, and $E_g$. This analysis based on thermal redistribution also allows us to extract values of parameters characterizing the low-energy electronic structure, which are in good agreement with those derived from density functional theory (DFT) calculations.

### A. Three-band model

To model thermal redistribution effects on the optical response, we consider the simplified three-band case shown in Fig. 1(d). We note that the *ab initio* calculation results in Fig. 5(a) suggest multiple conduction and valence bands near $E_F$ at both the $Y$ and Γ points. A large number of direct and indirect optical processes involving these bands are therefore anticipated. Similarly, thermal activation of hole states in the valence bands as well as electron states in the conduction bands might also be expected. In the interest of simplicity and of obtaining physical insight, we limit our model to a single valence band and two conduction bands. Figure 5(b) shows this simplified three-band electronic structure. We retain conduction bands at Y and Γ and a single, occupied valence band at Y. Given that $SrMnSb_2$ shows a Drude peak in $\sigma_1(\omega)$ at low $T$, we include a partially filled conduction band at Y. To explain the strong $T$-dependent direct optical transition in Fig. 2(b), we also include the valence band at Y. Finally, to account for the shift in $\omega_p$ at low $T$, we also include one more conduction band located at Γ. In principle, thermal activation of the hole states near Γ might also be relevant, but we neglect this process for simplicity. The simplified electronic structure of Fig. 5(b) can be parametrized by the offset between conduction-band minima ($\Delta$), the masses ($m_Y$ and $m_\Gamma$) of the Y and Γ bands, the separation $E_o$ between the conduction-band minimum and valence-band maximum at Y, and $E_F$. The value of $E_F$ is determined by the number of free carriers at zero $T$. We further assume that the relevant bands are quasi-2D, leading to the density of states [$D(E)$] schematically shown in Fig. 5(d).

Within the proposed three-band model, the important optical processes will be the Drude response and direct

band-to-band transitions. At $T = 0$, $\sigma_1(\omega)$ is dominated by two processes: an intraband (Drude) contribution involving electrons in the light Y band and direct interband transitions originating from the occupied Y valence band and terminating at $E_F$. The relevant interband optical transition is indicated with a arrow in Fig. 5(b). At finite $T$, indirect transitions from the valence band at Y to conduction band at Γ may also occur, but are expected to be much weaker compared to the direct transitions involving the light Y bands [22]. This is in accord with the 10 K optical data, shown in in Fig. 2(a), where only Drude and direct transition contributions are observed.

With increased $T$, there is a significant thermal redistribution of quasiparticles between the conduction bands that causes large changes in the optical response. The evolution of the electron occupancies at finite $T$ is depicted in Figs. 5(b)–5(d). As $T$ increases, the unoccupied Γ conduction band is progressively populated. As a result, the effective optical mass of the quasiparticles is increased due to the involvement of the heavy Γ states. Because of the highly structured $D(E)$ and small $E_F$, the chemical potential $\mu$ is strongly $T$ dependent and decreases as $T$ is raised. The effects of such population change can be dramatic, especially when the carrier density is small. These thermally driven band occupancy changes lead to a redshift of both $\omega_p$ and $E_g$, in accord with the optical data shown in Figs. 2 and 3. We note that similar reasoning has been invoked to explain optical and Hall data in doped PbTe, where a second, heavy valence band is thought to play an important role [27,43]. The thermal effect on the direct transitions is analogous to the well-known Moss-Burstein effect [44,45]. However, in this case, the shift is produced by $T$-dependent changes in $\mu$, rather than changes in $E_F$ due to chemical doping.

The effect of thermal redistribution between bands on the optical properties ($\omega_p$ and $E_g$) can be quantitatively accounted for in the three-band picture. By assuming a constant charge density ($n$), we self-consistently evaluate $\mu(T)$ using

$$n = \int_0^\infty D(E) f(\mu, E, T) dE, \tag{1}$$

where $D(E)$ is the total density of states shown in Fig. 5(d) and $f(\mu, E, T)$ is the Fermi-Dirac function. For simplicity, we assume that the density of states and transport masses are equal and define $\mu$ with respect to the $Y$ conduction-band edge. With $\mu(T)$ in hand, the carrier densities in the $Y$ band ($n_Y$) and in the Γ band ($n_\Gamma$) can be separately computed using

$$n_Y = \int_0^\infty D_Y(E) f(\mu, E, T) dE, \tag{2}$$

$$n_\Gamma = \int_0^\infty D_\Gamma(E) f(\mu, E, T) dE, \tag{3}$$

where $D_Y$ and $D_\Gamma$ are the band-resolved density of states. We emphasize that $n = n_Y + n_\Gamma$ is conserved at all $T$ in our analysis. Finally, $\omega_p$ and $E_g$ can be computed according to

$$\omega_p^2(T) = 4\pi e^2 [n_Y(T)/m_Y + n_\Gamma(T)/m_\Gamma] \tag{4}$$

and

$$E_g(T) = E_o + 2\mu(T). \tag{5}$$

Note that we have assumed that the squared plasma frequencies can be added (implying equal lifetime $\tau$ in each valley) and that the conduction-band and valence-band masses at Y are equal [yielding the factor of 2 in Eq. (5)].

### B. Comparison of three-band model with the optical data

We applied the three-band model to our data and could successfully explain the optical response of $SrMnSb_2$. The above procedure was performed using parameters suitable to $SrMnSb_2$. Specifically, we use $n = 2.84 \times 10^{19}\,\mathrm{cm}^{-3}$, $m_Y = 0.069\,m_e$, and $E_F = 116$ meV, following our earlier discussion in Sec. III. $E_o$ was set to 44 meV in order to match the low-$T$ $E_g$ value. We tried several values of Δ and $m_\Gamma/m_Y$ in order to best reproduce the optical data. The results of our calculations, together with the experimental data, are shown in Fig. 6. Importantly, the model calculation captures the redshift of both $\omega_p^2$ and $E_g$ with increasing $T$. As shown in Figs. 6(a) and 6(c), $\omega_p^2(T)$ is well reproduced with $\Delta = 141$ meV and $m_\Gamma/m_Y = 11$. On the other hand, these values lead to a slight overestimation of $E_g$ above 200 K, as can be seen in Figs. 6(b) and 6(d). This discrepancy is likely a result of other factors, such as thermal expansion of the lattice or the electron-phonon interaction [46], that are expected to further renormalize the optical gap at finite $T$ and are not included in our model. Nonetheless, our model suggests that the majority of the change in $E_g$ is driven by the change in $\mu$ caused by the multiband electronic structure near $E_F$.

The band structure parameter values obtained through our model analysis agree reasonably well with the DFT results shown in Fig. 5(a). The best agreement between the experimental data and model outputs was achieved when $m_\Gamma/m_Y = 11$, suggesting that the band mass difference between the two conduction bands of $SrMnSb_2$ is quite large. Further, $\Delta = 141$ meV indicates that the second conduction-band minimum is located close to $E_F$. Remarkably, these values of Δ and $m_\Gamma/m_Y$ compare favorably with the values of $\Delta_{DFT} \sim 116$ meV and $m_\Gamma/m_Y = 8.6$ derived from the DFT band structure. The parameters extracted from our analysis of the optical, Hall, and DFT results are summarized in Table I. The agreement between experiment and theory further validates our discussion and demonstrates that, combined with proper analysis, optical spectroscopy can provide a detailed probe of the near-$E_F$ electronic structure in low-carrier-density, multiband metals.

The three-band model also provides insight into how the electronic structure determines the anomalous optical response. For instance, the thermal effect on $\omega_p$ should become stronger as the mass difference between the two conduction bands, $m_\Gamma/m_Y$, is increased. As shown in Fig. 6(a), for various $m_\Gamma/m_Y$ ratios and fixed $\Delta = 141$ meV, $\omega_p^2$ is relatively constant at low $T$ before decreasing as $T$ is increased above 75 K. The magnitude of this effect, as well as the slope of the model curves far above 75 K, increases with increasing $m_\Gamma/m_Y$. In the special case of $m_\Gamma/m_Y = 1$, $\omega_p^2$ does not depend on $T$ as the Γ states contribute equally to the optical response. This demonstrates that for two bands with minimal mass difference, an anomalous $\omega_p^2(T)$ behavior should not be observed. Similarly, the magnitude of the shift of $E_g$ also depends on $m_\Gamma/m_Y$. Therefore, the anomalous $T$-dependent

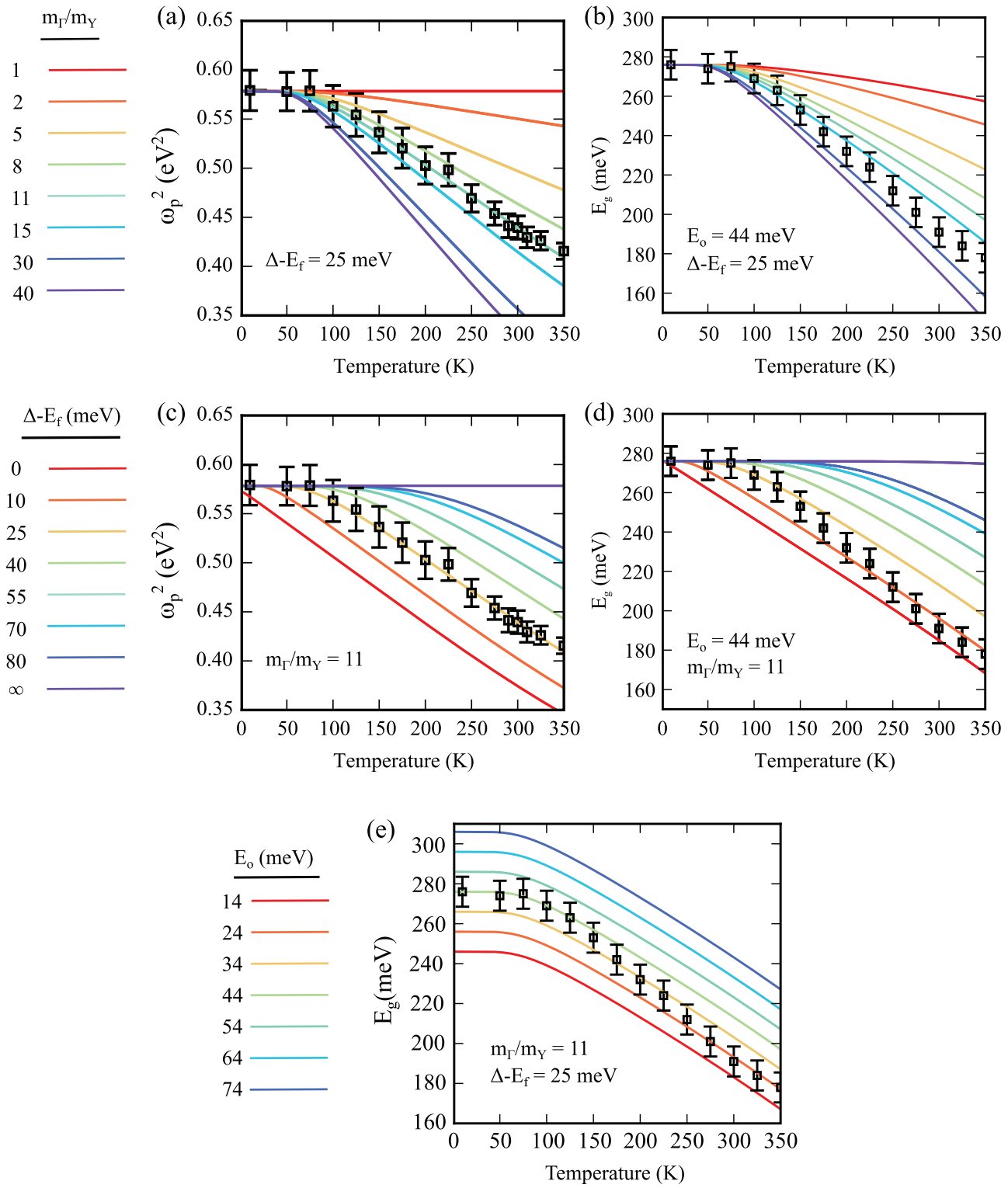


FIG. 6. Comparison between experimental and model optical properties. (a) $\omega_p^2(T)$ for various $m_\Gamma/m_Y$. (b) $E_g$ for various $m_\Gamma/m_Y$. (c) $\omega_p^2(T)$ for various $\Delta - E_F$. (d) $E_g$ for various $\Delta - E_F$. (e) $E_g$ for various $E_o$.

shift of $\omega_p$, observed in some other material systems [16], suggests that these materials may also have multiple bands with large effective mass differences near $E_F$.

The thermal effects on $\omega_p^2$ and $E_g$ should also be larger when the energy difference between the two conduction bands, $\Delta$, becomes comparable to $E_F$. The influence of $\Delta$ is illustrated in Figs. 6(c) and 6(d) for $E_F = 116$ meV, $m_\Gamma/m_Y = 11$, and $E_o = 44$ meV. Both $\omega_p^2$ and $E_g$ redshift as $T$ increases, in agreement with the experimental data. The $T$ at which this shift begins sensitively depends on $\Delta - E_F$. This demonstrates that the cusp (~75 K in the data) in $\omega_p^2(T)$ and $E_g(T)$ corresponds to the $T$ at which the heavy $\Gamma$ states begin to be populated.

TABLE I. Parameters obtained from our experimental studies ($n_{\text{total}}$, $\omega_p$), optimal fitting parameters ($E_F$, $\Delta$, $m_Y$ and $m_\Gamma$) and from DFT calculations ($\Delta$, $m_Y$ and $m_\Gamma$), characterizing the electronic structure of $SrMnSb_2$.

| Parameters | Experiments/model fitting | DFT calculation |
|---|---|---|
| $n$ (10 K) | $2.8 \times 10^{19}$ cm$^{-3}$ | |
| $\omega_p$ (10 K) | 0.76 eV | |
| $E_F$ | 116 meV | |
| $\Delta$ | 141 meV | 116 meV |
| $m_Y$ | 0.069 $m_e$ | 0.054 $m_e$ |
| $m_\Gamma$ | 0.76 $m_e$ | 0.47 $m_e$ |

We note that in the limiting case of $\Delta - E_F = \infty$ (effectively the single-conduction-band limit), neither $\omega_p^2$ nor $E_g$ display a $T$ dependence, suggesting no thermal excitation effects.

Finally, we can determine the separation between the conduction band minimum and valence-band maximum to be about 40 meV. Figure 6(e) shows the effect of varying $E_o$. As expected, $E_g$ is linearly proportional to the $E_o$ value. The best fitting can be obtained with $E_o \cong 44$ meV at least at low $T$. This value can be independently checked with Eq. (5): That is, the intrinsic gap $E_o = E_g(T = 0) - 2E_F$. $E_o$ is therefore uniquely determined by the low $T$ value of $E_g$, provided $E_F$ is known. With $E_g(T = 0) \cong 276$ meV and $E_F = 116$ meV, $E_o \cong 44$ meV.

### C. Analysis of Hall data

To further confirm our interpretation, we also calculated the $T$-dependent Hall data based on the three-band model. The obtained values of $E_F = 116$ meV and $\Delta = 141$ meV are much larger than $k_B T$. We therefore employ a two-conduction-band model developed for $Pb_{1-x}Sn_xTe$ [43]. In this model, $R_H$ is given by

$$R_H = (1/e)(\gamma n_\Gamma + n_Y b^2)/(n_\Gamma + n_Y b)^2, \quad (6)$$

where $b$ is the ratio of the mobilities of the two bands and $\gamma$ is the Hall factor which we set to unity. For simplicity, we assume identical lifetimes in each band so that $b = m_Y/m_\Gamma$. The resulting $R_H$ values, computed using several parameter sets, are shown in Fig. 7 together with the experimental results. In the special case of $m_\Gamma/m_Y = 1$, $R_H$ is $T$ independent, as is evident from Eq. (6). As shown in Fig. 7(a), the high-$T$ slope depends strongly on $m_\Gamma/m_Y$. In Fig. 7(b), the location of the "cusp" in $R_H$ is seen to be sensitive to the choice of $\Delta$, similar to the model optical properties.

We found that the $T$ dependence of the Hall data can also be explained reasonably within the three-band model. Consistent with the experimental data, the calculated $R_H$ is relatively constant below 50 K, at which point it begins to rise quasilinearly. As mentioned earlier, the optical data are well described by $\Delta = 141$ meV and $m_\Gamma/m_Y = 11$. However, with these parameter values, the three-band model tends to underestimate the experimental value of $R_H$ by about 10% at higher temperatures. This discrepancy could arise for several reasons. First, we have ignored $T$-dependent changes in the mobility ratio [$b$ in Eq. (6)] or in the overall band structure. Second, we have not considered possible contributions from

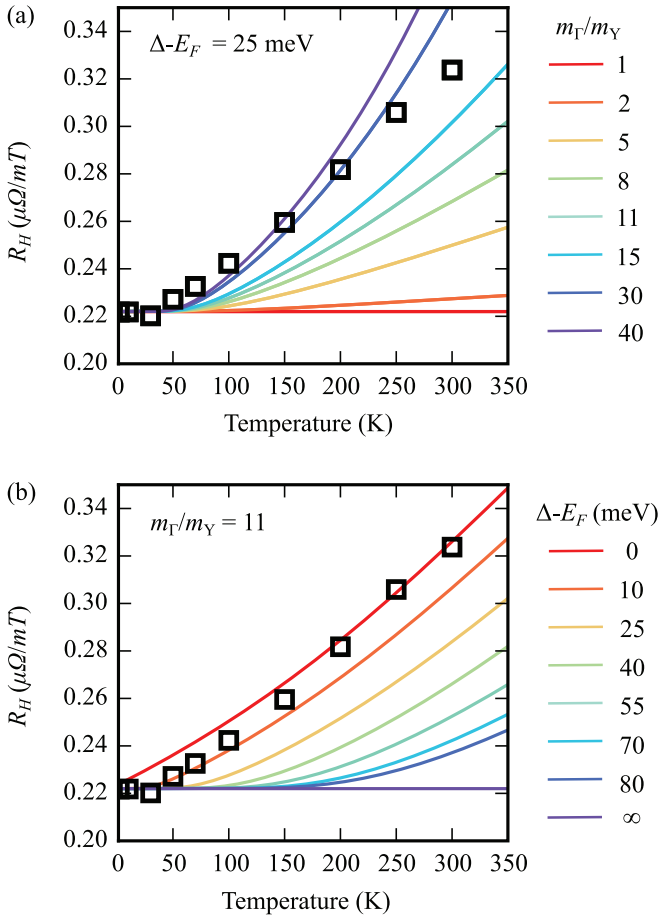


FIG. 7. Comparison between experimental and model Hall number ($R_H$). (a) Effect of varying $m_\Gamma/m_Y$. (b) Effect of varying $\Delta - E_F$.

bands beyond the conduction bands at $\Gamma$ and $Y$. At finite temperatures, other carriers, such as thermally activated holes in the valence band near $\Gamma$ [Fig. 5(a)], may become relevant. Given these considerations, we regard the Hall data to be in good agreement with both the optical data and the schematic band structure shown in Fig. 5(a).

## IV. APPLICABILITY TO OTHER MATERIALS AND CONCLUSIONS

The above discussion demonstrates that large changes in $\omega_p$ can arise from simple thermal and band structural effects that could be important in a variety of materials. The key requirements are an effective mass that varies significantly within a few tens of meV of the Fermi level (corresponding to experimentally accessible temperatures) and a small Fermi energy. In the case of $SrMnSb_2$, we have shown that the variation in mass is a result of a nearby heavy band, but this condition might also be satisfied by, for instance, strong nonparabolicity. Indeed, a $T$-dependent optical mass has been identified in $Pb_{1-x}Sn_xTe$ and explained as a consequence of strong band nonparabolicity and, at higher carrier densities, of a second band near $E_F$ [27,47]. We therefore expect that this effect should be active in a variety of low-carrier-density metals.

In fact, available optical data support the general applicability of our results. For example, $Cu_xTiSe_2$, which shows an

anomalous $T$ dependence of $\omega_p$, is a low-carrier-density metal with a complex, multiband electronic structure [16]. Similar physics to what we have described in $SrMnSb_2$ may apply in this compound. Furthermore, several topological insulator materials also show increases in $\omega_p$ with $T$ [17,18]. These should be considered metallic, doped semiconductors with small Fermi energies and highly structured density of states near the Fermi level. For instance, the DFT band structure of $Bi_2Se_3$ reveals a bulk conduction-band minimum at $\Gamma$, with additional valleys within about 0.3 eV [48]. In particular, a valley located near L involves weakly dispersing states that should yield a large optical band mass. This is qualitatively similar to the case of $SrMnSb_2$ and the thermal activation of heavy L states therefore provides a natural explanation for the $T$-dependent shifts in $\omega_p$ observed in the Bi-based topological insulator materials, although nonparabolicity may also be important to these materials. We mention that certain lead chalcogenide thermoelectric alloys, similar to PbTe, also show temperature-dependent optical masses, possibly due to nonparabolic or multiband electronic structures [19,20]. Lastly, we note that a strongly $T$-dependent $\omega_p$ was also observed in metallic $LaTiO_3/SrTiO_3$ superlattices [21]. This observation was reasonably interpreted in terms of the leakage of electrons across the LTO/STO interface dictated by the quantum paraelectric behavior of STO. However, the $t_{2g}$ bands in these compounds should be quasidegenerate, favoring a multiband electronic structure near $E_F$ [49] and there are also indications of multichannel conduction from magnetotransport experiments [50]. We therefore suggest that multiband effects may also be important in determining the $T$-dependent optical and transport properties of LTO/STO superlattices and, by extension, other varieties of oxide heterostructures.

## V. SUMMARY

We have studied the optical response of $SrMnSb_2$. Most importantly, we observed a strikingly large increase in $\omega_p$ at low temperatures, as well as concurrent changes in the optical interband transitions and Hall data. This behavior was shown to be a consequence of the multiband electronic structure and small $E_F$ in $SrMnSb_2$. At high temperatures, heavier states lying close to $E_F$ become thermally populated, leading to a reduction in $\omega_p$. We expect that this effect could be relevant to understanding the transport properties of a number of topical low-carrier-density and multiband metals.

## ACKNOWLEDGMENTS

This work was supported by the Research Center Program of the Institute for Basic Science in Korea (Grant No. IBS-R009-D1). S.J.M. was supported by Basic Science Research Program through the National Research Foundation of Korea (NRF) funded by the Ministry of Science, ICT and Future Planning (Grant No. 2014R1A2A1A11054351). J.H.S. was supported by Nano Material Technology Development Program (Green Nano Technology Development Program) through the National Research Foundation of Korea (NRF) funded by the Ministry of Education, Science and Technology (Grant No. 2011-0030146).

H. J. Park and Luke J. Sandilands are equally contributed in this work.

## APPENDIX A: THE SINGLE-BAND DRUDE MODEL

Here we review the single-band Drude model that is commonly used to understand the optical properties of a metal. In the Drude model, the dielectric function, $\tilde{\varepsilon}$ $(= 1 + 4\pi i\tilde{\sigma}/\omega)$, is given by

$$\tilde{\varepsilon} = \varepsilon_1 + i\varepsilon_2 = \varepsilon_\infty - \frac{\omega_p^2}{\omega^2 + i\omega(1/\tau)}. \tag{A1}$$

Here $\varepsilon_\infty$ is a dielectric constant that represents screening due to higher-energy interband transitions, $\omega_p$ is the quasiparticle plasma frequency, and $1/\tau$ is the scattering rate. Importantly, for the single-band case, $\omega_p^2 = 4\pi e^2 n/m_b$, where $n$ is the quasiparticle density and $m_b$ the optical effective mass [22]. Therefore, optical spectroscopic studies using the single-band Drude model have provided a simple and powerful platform for understanding the optical response of a metal and for relating this response to electrodynamic parameters such as $\omega_p$, $\varepsilon_\infty$, and $1/\tau$.

The Drude model suggests that a metallic system should have several characteristic features. In the limit of $\omega_p/\varepsilon_\infty^{1/2} \gg 1/\tau$ and $\omega \gg 1/\tau$, Eq. (A1) can be written as

$$\varepsilon_1 \cong \varepsilon_\infty - \frac{\omega_p^2}{\omega^2}. \tag{A2}$$

The Drude model therefore predicts a characteristic zero crossing in $\varepsilon_1$ at the screened plasma frequency $\omega_p^* = (\omega_p/\varepsilon_\infty^{1/2})$. At energies far below $\omega_p^*$, $\varepsilon_1$ is large and negative. Far above $\omega_p^*$, $\varepsilon_1$ approaches $\varepsilon_\infty$. Meanwhile, the Drude model $\sigma_1(\omega)$ consists of a peak at $\omega = 0$ with a width given by $1/\tau$ and an intensity determined by $\omega_p^2$. These characteristics lead to several well-defined spectroscopic features in the optical response (e.g., $R(\omega) = |[1 - \tilde{\varepsilon}(\omega)^{1/2}]/[1 + \tilde{\varepsilon}(\omega)^{1/2}]|^2$. For instance, $R(\omega)$ is expected to be large at low energies before reaching a minimum, known as the plasma edge, at $\omega_p^*$ before increasing up to a constant value determined by $\varepsilon_\infty$. The plasma edge is a signature of metallic transport and is often used to determine $\omega_p^*$ [51].

The Drude model also allows for various methods of quantifying the bare plasma frequency $\omega_p$. First, $\omega_p$ can be evaluated through direct integration of the Drude peak via the optical sum rule,

$$\omega_p^2 = 8\int \sigma_1^D(\omega)d\omega, \tag{A3}$$

where $\sigma_1^D(\omega)$ is the Drude contribution to $\sigma_1(\omega)$ [22]. A second route is via the longitudinal loss function [$\mathrm{Im}(-1/\varepsilon)$]. Within the Drude model, $\mathrm{Im}(-1/\varepsilon)$ can be written by

$$\mathrm{Im}(-1/\varepsilon) = \frac{\omega_P^2\,\omega/\tau}{\varepsilon_\infty^2\omega^2/\tau^2 + \left(\omega_P^2 - \varepsilon_\infty\omega^2\right)^2}. \tag{A4}$$

Contrary to the Drude peak in $\sigma_1(\omega)$, which is located at zero frequency, the Drude model predicts that this peak should be located close to $\omega_p^*$. Equation (A4) is therefore a useful alternative when $\sigma_1(\omega)$ cannot be determined accurately at

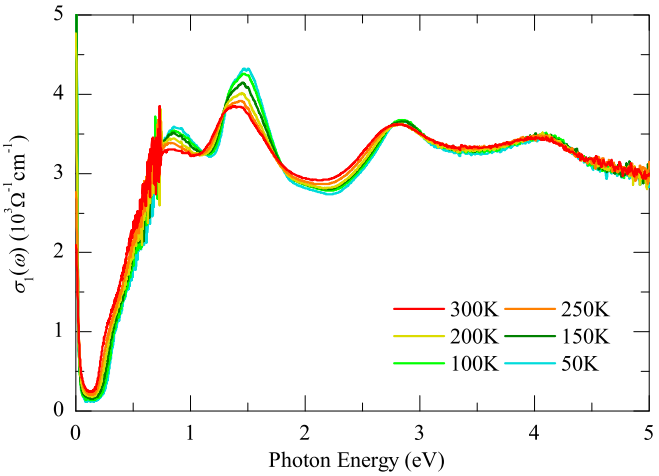


FIG. 8. Temperature-dependent $\sigma_1(\omega)$ over a broad energy range.

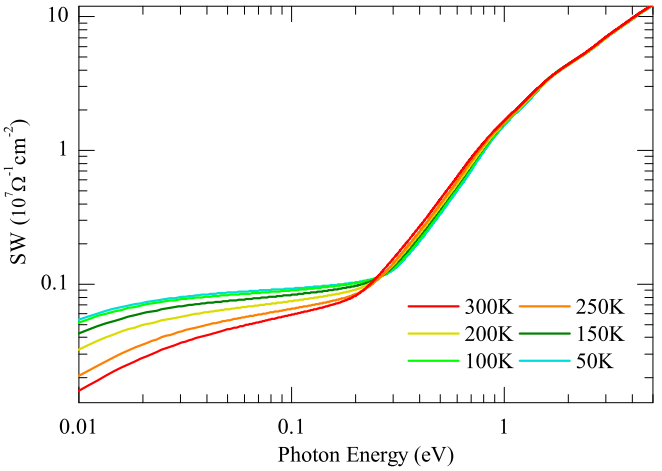


FIG. 9. Temperature-dependent spectral weight (SW) over a broad energy range.

low frequencies. Finally, the location of the zero crossing in $\varepsilon_1$, as suggested by Eq. (A2), can also be used to determine $\omega_p^*$. More generally, from Eq. (A1), the zero crossing frequency $\omega_{\text{zero}}$ should occur at $(\omega_p^{*2} - 1/\tau^2)^{1/2}$, so

$$\omega_p^{*2} = \omega_{\text{zero}}^2 + 1/\tau^2. \tag{A5}$$

When $1/\tau$ is much smaller than $\omega_p^*$, $\omega_{\text{zero}}$ corresponds to $\omega_p^*$, as expected from Eq. (A2). However, when $1/\tau$ becomes larger, $\omega_{\text{zero}}$ will underestimate the true $\omega_p^*$.

## APPENDIX B: SPECTRAL WEIGHT CONSERVATION

We show temperature-dependent $\sigma_1(\omega)$ and the spectral weight [SW $= \int_0^{\omega} \sigma_1(\omega')d\omega'$] in the energy region up to 5 eV in Fig. 8. The conductivity below 0.25 eV is dominated by a Drude response. Conspicuous interband transitions are observed at 0.8, 1.5, 2.8, and 4 eV. As the temperature increases, the interband transitions become broader and redshifted.

Our spectral weight analysis in a wide energy region shows that the spectral weight lost from the Drude is recovered at about 250 meV which corresponds to the onset of the lowest interband transition (Fig. 9). This indicates that the changes in the Drude response with the variation in temperature mostly involve the interband transitions located in the energy region below 250 meV. The thermal broadening and redshift of the interband transitions lead to a minor variation in the spectral weight in the energy region between 250 meV and 3 eV and the spectral weight is conserved above 3 eV.


[1] X. Du, S.-W. Tsai, D. L. Maslov, and A. F. Hebard, Phys. Rev. Lett. **94**, 166601 (2005).

[2] Z. Zhu, A. Collaudin, B. Fauque, W. Kang, and K. Behnia, Nat. Phys. **8**, 89 (2012).

[3] A. H. Castro Neto, F. Guinea, N. M. R. Peres, K. S. Novoselov, and A. K. Geim, Rev. Mod. Phys. **81**, 109 (2009).

[4] M. Z. Hasan and C. L. Kane, Rev. Mod. Phys. **82**, 3045 (2010).

[5] S. M. Young, S. Zaheer, J. C. Y. Teo, C. L. Kane, E. J. Mele, and A. M. Rappe, Phys. Rev. Lett. **108**, 140405 (2012).

[6] H. Weng, C. Fang, Z. Fang, B. A. Bernevig, and X. Dai, Phys. Rev. X **5**, 011029 (2015).

[7] Z. K. Liu, J. Jiang, B. Zhou, Z. J. Wang, Y. Zhang, H. M. Weng, D. Prabhakaran, S. K. Mo, H. Peng, P. Dudin, T. Kim, M. Hoesch, Z. Fang, X. Dai, Z. X. Shen, D. L. Feng, Z. Hussain, and Y. L. Chen, Nat. Mater. **13**, 677 (2014).

[8] S. A. Parameswaran, T. Grover, D. A. Abanin, D. A. Pesin, and A. Vishwanath, Phys. Rev. X **4**, 031035 (2014).

[9] J. Xiong, S. K. Kushwaha, T. Liang, J. W. Krizan, W. Wang, R. J. Cava, and N. P. Ong, arXiv:1503.08179v1.

[10] P. J. Moll, N. L. Nair, T. Helm, A. C. Potter, I. Kimchi, A. Vishwanath, and J. G. Analytis, arXiv:1505.02817v2.

[11] S.-Y Xu, I. Belopolski, N Alidoust, M. Neupane, G Bian, C. Zhang, R. Sankar, G. Chang, Z. Yuan, C.-C. Lee, S-M. Huang, H. Zheng, J. Ma, D S. Sanchez, B. Wang, A. Bansil, F. Chou, P. P. Shibayev, H. Lin, S. Jia *et al.*, Science **349**, 613 (2015).

[12] H. Cercellier, C. Monney, F. Clerc, C. Battaglia, L. Despont, M. G. Garnier, H. Beck, P. Aebi, L. Patthey, H. Berger, and L. Forró, Phys. Rev. Lett. **99**, 146403 (2007).

[13] P. J. Hirschfeld, M. M. Korshunov, and I. I. Mazin, Rep. Prog. Phys. **74**, 124508 (2011).

[14] Y. Lubashevsky, E. Lahoud, K. Chashka, D. Podolsky, and A. Kanigel, Nat. Phys. **8**, 309 (2012).

[15] S. Kasahara, T. Watashige, T. Hanaguri, Y. Kohsaka, T. Yamashita, Y. Shimoyama, Y. Mizukami, R. Endo, H. Ikeda, K. Aoyama, T. Terashima, S. Uji, T. Wolf, H. von Löhneysen, T. Shibauchi, and Y. Matsuda, Proc. Natl. Acad. Sci. USA **111**, 16309 (2014).

[16] G. Li, W. Z. Hu, J. Dong, D. Qian, D. Hsieh, M. Z. Hasan, E. Morosan, R. J. Cava, and N. L. Wang, Phys. Rev. Lett. **99**, 167002 (2007).

[17] S. V. Dordevic, M. S. Wolf, N. Stojilovic, H. Lei, and C. Petrovic, J Phys.: Condens. Matter **25**, 075501 (2013).

[18] T. Dong, R.-H. Yuan, Y.-G. Shi, and N.-L. Wang, Chin. Phys. Lett. **30**, 127801 (2013).
[19] N. Anand, S. Buvaev, A. F. Hebard, D. B. Tanner, Z. Chen, Z. Li, K. Choudhary, S. B. Sinnott, G. Gu, and C. Martin, Phys. Rev. B **90**, 235143 (2014).
[20] A. A. Reijnders, J. Hamilton, V. Britto, J.-B. Brubach, P. Roy, Q. D. Gibson, R. J. Cava, and K. S. Burch, Phys. Rev. B **90**, 235144 (2014).
[21] S. S. A. Seo, W. S. Choi, H. N. Lee, L. Yu, K. W. Kim, C. Bernhard, and T. W. Noh, Phys Rev. Lett. **99**, 266801 (2007).
[22] M. Dressel and G. Grüner, *Electrodynamics of Solids: Optical Properties of Electrons in Matter* (Cambridge University Press, New York, 2002).
[23] D. N. Basov, R. D. Averitt, D. van der Marel, M. Dressel, and K. Haule, Rev. Mod. Phys. **83**, 471 (2011).
[24] C. C. Homes, Y. M. Dai, J. S. Wen, Z. J. Xu, and G. D. Gu, Phys. Rev. B **91**, 144503 (2015).
[25] C. C. Homes, M. N. Ali, and R. J. Cava, Phys. Rev. B **92**, 161109(R) (2015).
[26] D. Wu, N. Barišić, P. Kallina, A. Faridian, B. Gorshunov, N. Drichko, L. J. Li, X. Lin, G. H. Cao, and Z. A. Xu, Phys. Rev. B **81**, 100512 (2010).
[27] J. R. Dixon and H. R. Riedl, Phys. Rev. **138**, A873 (1965).
[28] J. Park, G. Lee, F. Wolff-Fabris, Y. Y. Koh, M. J. Eom, Y. K. Kim, M. A. Farhan, Y. J. Jo, C. Kim, J. H. Shim, and J. S. Kim, Phys. Rev. Lett. **107**, 126402 (2011).
[29] Y. Feng, Z. Wang, C. Chen, Y. Shi, Z. Xie, H. Yi, A. Liang, S. He, J. He, Y. Peng, X. Liu, Y. Liu, L. Zhao, G. Liu, X. Dong, J. Zhang, C. Chen, Z. Xu, X. Dai, Z. Fang *et al.*, Sci. Rep. **4**, 5385 (2014).
[30] J. K. Wang, L. L. Zhao, Q. Yin, G. Kotliar, M. S. Kim, M. C. Aronson, and E. Morosan, Phys. Rev. B **84**, 064428 (2011).
[31] G. Lee, M. A. Farhan, J. S. Kim, and J. H. Shim, Phys. Rev. B **87**, 245104 (2013).
[32] J. H. Shim, K. Haule, and G. Kotliar, Phys. Rev. B **79**, 060501 (2009).
[33] L. Degiorgi, A. V. Sologubenko, H. R. Ott, F. Drymiotis, and Z. Fisk, Phys. Rev. B **65**, 041101 (2001).
[34] K. Wang, D. Graf, H. Lei, S. W. Tozer, and C. Petrovic, Phys. Rev. B **84**, 220401 (2011).
[35] M. A. Farhan, G. Lee, and J. H. Shim, J. Phys.: Condens. Matter **26**, 042201 (2014).
[36] C. C. Homes, M. Reedyk, D. Cradles, and T. Timusk, Appl. Opt. **32**, 2976 (1993).
[37] M. Ortolani, P. Calvani, and S. Lupi, Phys. Rev. Lett. **94**, 067002 (2005).
[38] Y. M. Dai, A. Akrap, J. Schneeloch, R. D. Zhong, T. S. Liu, G. D. Gu, Q. Li, and C. C. Homes, Phys. Rev. B **90**, 121114 (2014).
[39] L. Degiorgi, E. Felder, H. R. Ott, J. L. Sarrao, and Z. Fisk, Phys. Rev. Lett. **79**, 5134 (1997).
[40] J. E. Hirsch, Phys Rev. B **62**, 14131 (2000).
[41] E. J. Singley, K. S. Burch, R. Kawakami, J. Stephens, D. D. Awschalom, and D. N. Basov, Phys. Rev. B **68**, 165204 (2003).
[42] J. S. Kim (unpublished).
[43] M. Ocio, Phys. Rev. B **10**, 4274 (1974).
[44] E. Burstein, Phys. Rev. **93**, 632 (1954).
[45] T. S. Moss, Proc. Phys. Soc., London, Sect. B **67**, 775 (1954).
[46] H. Ünlü, Solid-State Electron. **35**, 1343 (1992).
[47] H. A. Lyden, Phys. Rev. **135**, A514 (1964).
[48] H. Zhang, C.-X. Liu, X.-L. Qi, X. Dai, Z. Fang, and S.-C. Zhang, Nat. Phys. **5**, 438 (2009).
[49] F. Lechermann, L. Boehnke, and D. Grieger, Phys. Rev. B **87**, 241101 (2013).
[50] J. S. Kim, S. S. A. Seo, M. F. Chisholm, R. K. Kremer, H. U. Habermeier, B. Keimer, and H. N. Lee, Phys. Rev. B **82**, 201407 (2010).
[51] L. J. Sandilands, A. A. Reijnders, M. Kriener, K. Segawa, S. Sasaki, Y. Ando, and K. S. Burch, Phys. Rev. B **90**, 094503 (2014).